



This is a repository copy of *Persistent DNA damage alters the neuronal transcriptome suggesting cell cycle dysregulation and altered mitochondrial function.*

White Rose Research Online URL for this paper:
<https://eprints.whiterose.ac.uk/178513/>

Version: Published Version

Article:

Vazquez-Villasenor, I., Garwood, C.J., Simpson, J.E. orcid.org/0000-0002-3753-4271 et al. (3 more authors) (2021) Persistent DNA damage alters the neuronal transcriptome suggesting cell cycle dysregulation and altered mitochondrial function. *European Journal of Neuroscience*, 54 (9). pp. 6987-7005. ISSN 0953-816X

<https://doi.org/10.1111/ejn.15466>

Reuse

This article is distributed under the terms of the Creative Commons Attribution (CC BY) licence. This licence allows you to distribute, remix, tweak, and build upon the work, even commercially, as long as you credit the authors for the original work. More information and the full terms of the licence here:
<https://creativecommons.org/licenses/>

Takedown

If you consider content in White Rose Research Online to be in breach of UK law, please notify us by emailing eprints@whiterose.ac.uk including the URL of the record and the reason for the withdrawal request.



eprints@whiterose.ac.uk
<https://eprints.whiterose.ac.uk/>

Persistent DNA damage alters the neuronal transcriptome suggesting cell cycle dysregulation and altered mitochondrial function

Irina Vazquez-Villasenor  | Claire J. Garwood  | Julie E. Simpson  |
Paul R. Heath  | Heather Mortiboys  | Stephen B. Wharton 

Sheffield Institute for Translational Neuroscience, The University of Sheffield, Sheffield, UK

Correspondence

Irina Vazquez-Villasenor, Sheffield Institute for Translational Neuroscience, The University of Sheffield, Sheffield, UK.
Email: i.vazquez@sheffield.ac.uk

Funding information

Medical Research Council, Grant/Award Number: MR/J004308/1; Alzheimer's Research UK, Grant/Award Number: PG2019A-003; Consejo Nacional de Ciencia y Tecnología; México: Fellow No. 217532

Edited by: Dr. Tara Spires-Jones

Abstract

Oxidative DNA damage induces changes in the neuronal cell cycle and activates a DNA damage response (DDR) to promote repair, but these processes may be altered under a chronic oxidative environment, leading to the accumulation of unrepaired DNA damage and continued activation of a DDR. Failure to repair DNA damage can lead to apoptosis or senescence, which is characterized by a permanent cell cycle arrest. Increased oxidative stress and accumulation of oxidative DNA damage are features of brain ageing and neurodegeneration, but the effects of persistent DNA damage in neurons are not well characterized. We developed a model of persistent oxidative DNA damage in immortalized post-mitotic neurons in vitro by exposing them to a sublethal concentration of hydrogen peroxide following a 'double stress' protocol and performed a detailed characterization of the neuronal transcriptome using microarray analysis. Persistent DNA damage significantly altered the expression of genes involved in cell cycle regulation, DDR and repair mechanisms, and mitochondrial function, suggesting an active DDR response to replication stress and alterations in mitochondrial electron transport chain. Quantitative polymerase chain reaction (qPCR) and functional validation experiments confirmed hyperactivation of mitochondrial Complex I in response to persistent DNA damage. These changes in response to persistent

Abbreviations: AU, arbitrary units; bFGF, basic fibroblast growth factor; BSA, bovine serum albumin; cRNA, complimentary RNA; DDR, DNA damage response; DE, differentially expressed; DMEM, Dulbecco's modified Eagle's medium; DMF, dimethyl formamide; DSBs, double-strand breaks; ds-cDNA, double-stranded cDNA; DSL, double-stressed LUHMES; FC, fold change; GCOS, Gene Chip Operating System; GDNF, glial-derived neurotrophic factor; H₂O₂, hydrogen peroxide; HDR, homology directed repair; IMPaLA, Integrated Molecular Pathway Level Analysis; iNeurons, directly reprogrammed patient-derived neurons; IVT, In Vitro Transcription; LUHMES, Lund Human Mesencephalic cell line; MCI, mild cognitive impairment; Mdivi-1, mitochondrial-division inhibitor 1; MTT, 3-(4,5-dimethylthiazol-2-yl)-2,5-diphenyltetrazolium bromide; NHEJ, non-homologous end-joining; OGD, oxygen glucose deprivation; PD, Parkinson's disease; PFA, paraformaldehyde; PLO, poly-L-ornithine; RMA, Robust Multi-Array Average; ROS, reactive oxygen species; RT, room temperature; SDS, sodium dodecyl sulphate; SEM, standard error of the mean; SSA, single strand annealing; SSL, single-stressed LUHMES; TCA, tricarboxylic acid; Tet, tetracycline hydrochloride; UDCA, ursodeoxycholic acid.

This is an open access article under the terms of the Creative Commons Attribution License, which permits use, distribution and reproduction in any medium, provided the original work is properly cited.

© 2021 The Authors. *European Journal of Neuroscience* published by Federation of European Neuroscience Societies and John Wiley & Sons Ltd.

oxidative DNA damage may lead to further oxidative stress, contributing to neuronal dysfunction and ultimately neurodegeneration.

KEYWORDS

cell cycle re-entry, DNA damage response, mitochondrial Complex I, oxidative stress, post-mitotic

1 | INTRODUCTION

Neurons are long-lived terminally differentiated cells that are particularly vulnerable to oxidative stress due to their high metabolic rate and limited antioxidant mechanisms (Dringen et al., 1999, 2005). Reactive oxygen species (ROS) are highly reactive molecules that can induce DNA damage in different ways, including the formation of double-strand breaks (DSBs), one of the most lethal forms of DNA damage (Sharma et al., 2016). Increased levels of oxidative stress and oxidative DNA damage have been described in the ageing brain and are hallmarks of neurodegeneration (Al-Mashhadi et al., 2015; Lu et al., 2004). Oxidative DNA damage is present in patients with mild cognitive impairment (MCI) and early Alzheimer's disease (AD), as well as in Parkinson's disease (PD) and amyotrophic lateral sclerosis (ALS) (Bradley-Whitman et al., 2014; Ferrante et al., 1997; Isobe et al., 2010; Murata et al., 2008; Shanbhag et al., 2019; Simpson et al., 2015).

To repair and prevent the effects of oxidative stress-induced DNA damage, neurons have evolved a DNA damage response (DDR) that is closely linked to cell cycle regulatory mechanisms. Despite the post-mitotic nature of neurons, cell cycle re-entry is a requirement for a DDR to be initiated in response to neuronal DNA damage under normal conditions (Kruman et al., 2004; Schwartz et al., 2007; Tomashevski et al., 2010). Persistent accumulation of oxidative DNA damage in neurodegenerative pathologies has also been shown to induce sustained activation of DDR signalling, which could initially be activated in order to promote repair, but that could become faulty or detrimental with chronicity (Barrio-Alonso et al., 2018; Kim et al., 2020; Silva et al., 2014; Simpson et al., 2015).

Persistent oxidative DNA damage can lead to aberrant cell cycle progression, genome instability, altered transcription and defective protein synthesis, but the involvement of these mechanisms in neurodegeneration has not been fully described. A persistent DDR is linked to oxidative damage in neurons from patients with cognitive impairment but with little or no AD-type pathology (Simpson et al., 2015); moreover, gene expression analysis of isolated neurons from these cases suggested that a

persistent DDR significantly changes the neuronal transcriptomic profile (Simpson et al., 2016). If the DNA damage is not completely repaired, resulting in a persistent DDR, it could also result in a senescent-like phenotype in neurons, a mechanism that was thought to only occur in mitotic cells (Jurk et al., 2012; Simpson et al., 2015). These data point to the involvement of persistent DNA damage and a DDR in the early stages of neurodegeneration, and a more detailed characterization is needed to identify their impact on neuronal function.

Transcriptome profiling is widely used to investigate gene expression patterns and allows the study of biological processes at the messenger RNA level under specific cellular conditions. Microarray has been successfully used to study gene expression changes in cultured cells and human tissue following already established and reproducible protocols (Ajikumar et al., 2019; Fadul et al., 2020; Ratcliffe et al., 2018; Simpson et al., 2011, 2016). To determine how persistent oxidative DNA damage affects neurons and could potentially lead to neuronal dysfunction, we developed an *in vitro* model of persistent oxidative stress in immortalized post-mitotic neurons and conducted transcriptomic profiling using microarray technology to determine alterations of cell pathways under this condition.

2 | MATERIALS AND METHODS

2.1 | LUHMES cell culture and oxidative DNA damage model

The Lund Human Mesencephalic (LUHMES, ATCC[®] CRL-2927[™]) cell line is a commercially available conditionally immortalized cell line derived from the tetracycline-controlled, v-myc-overexpressing human mesencephalic cell line MESC2.10 (Lotharius, 2005; Lotharius et al., 2002). Differentiation of LUHMES was performed following the two-step protocol previously established (Scholz et al., 2011) with some modifications. Base culture medium consisted of advanced Dulbecco's modified Eagle's medium (DMEM)/F12 (Gibco), 1× N2-Supplement (ThermoFisher Scientific), 2-mM L-glutamine (Lonza) and 1% penicillin/streptomycin

(Lonza). Proliferation medium consisted of base medium supplemented with 40 ng/ml recombinant basic fibroblast growth factor (bFGF) (Peprotech EC Ltd.); differentiation medium consisted of base medium supplemented with 2 ng/ml recombinant human glial-derived neurotrophic factor (GDNF) (Peprotech EC Ltd.) and 1 μ g/ml tetracycline hydrochloride (Tet) (Sigma-Aldrich). Proliferating LUHMES were cultured in T75 coated flasks in proliferation medium until cells reached 70%–80% confluency, with a media change every 2 days. To start differentiation, confluent proliferating LUHMES were cultured in differentiation medium, and 2 days after, pre-differentiated LUHMES were trypsinized, replated on to the appropriate coated plates at 2.5×10^5 cells/cm² and cultured in differentiation medium for a further 3 days. To confirm successful generation of post-mitotic LUHMES, expression of morphological changes and decline in the expression of proliferation markers was

assessed throughout the differentiation protocol, which lasts a total of 5 days (Figure S1). All experiments were performed on Day 6, at which point LUHMES were considered to be post-mitotic. Cell culture flasks, multiwell plates and glass coverslips used for LUHMES culture were coated at 37°C for ≥ 3 h with 50 μ g/ml poly-L-ornithine (PLO) hydrobromide and 1 μ g/ml fibronectin from human plasma (both from Sigma-Aldrich, St Louis, MO, USA) in distilled water (dH₂O).

2.2 | Induction of oxidative DNA damage in post-mitotic LUHMES and cell viability assessment

To induce oxidative DNA damage, differentiated LUHMES were incubated either once (single-stressed LUHMES [SSL]) or twice (double-stressed LUHMES

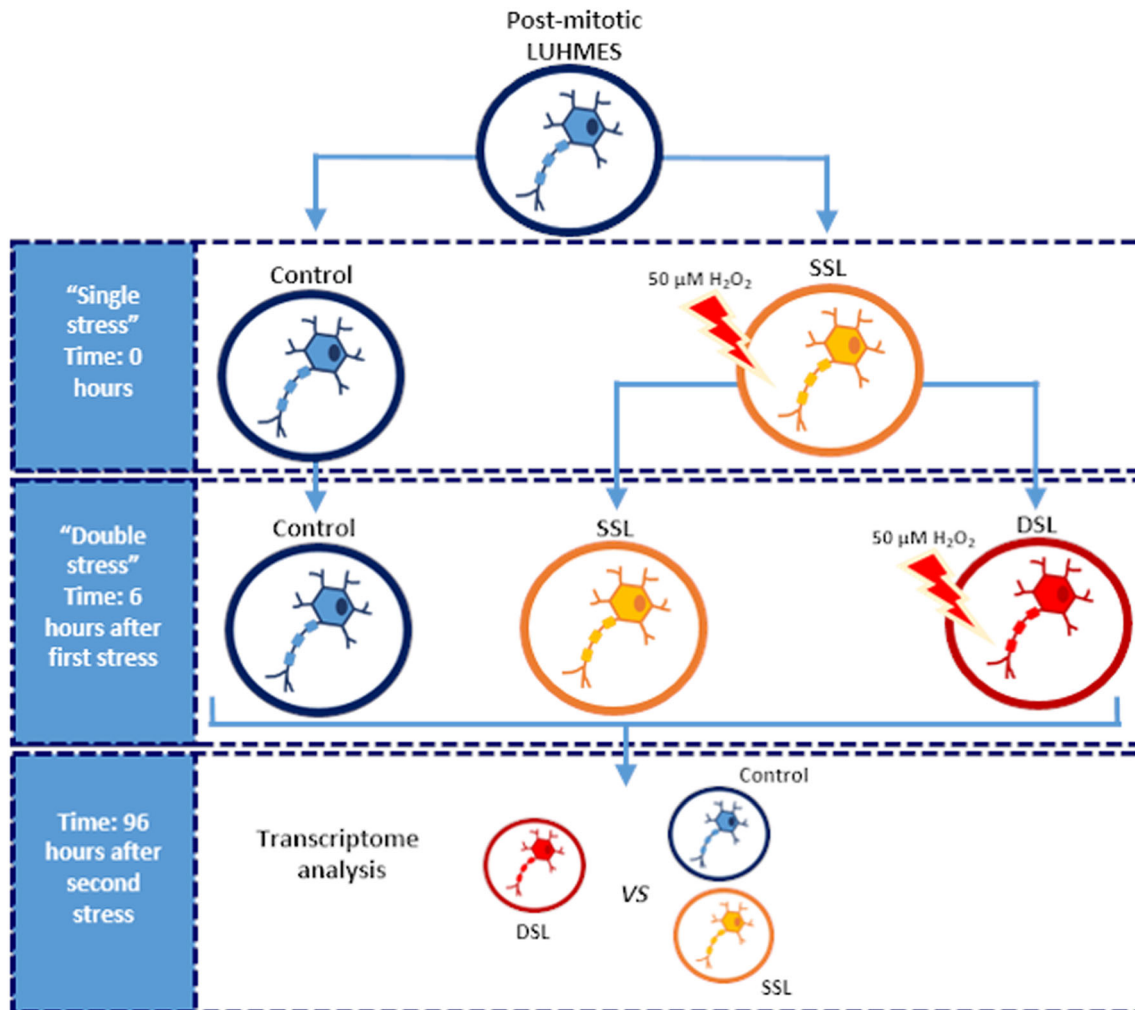


FIGURE 1 Double-stress protocol followed to induce persistent oxidative DNA damage in human neurons in vitro. Differentiated LUHMES (sixth day of differentiation) were stressed with 50- μ M H₂O₂. Six hours after the first stress, cells were exposed to a second 50- μ M H₂O₂ challenge (DSL), whereas only the vehicle was added to control and single-stressed LUHMES (SSL). Changes in the transcriptome of control, SSL and DSL were assessed 96 h after exposure to the second 50- μ M H₂O₂ stress

[DSL]) with 50- μ M hydrogen peroxide (H_2O_2); the second 50- μ M H_2O_2 stress was added to the culture medium 6 h after the first one. Vehicle only (dH_2O) was added to control LUHMES, and cells were then cultured for a further 96 h with one media change at 48 h (Figure 1). The concentration of 50- μ M H_2O_2 was selected based on preliminary experiments that assessed cell viability of post-mitotic LUHMES exposed to increasing concentrations of H_2O_2 (Figure S2).

The MTT (3-(4,5-dimethylthiazol-2-yl)-2,5-diphenyltetrazolium bromide) reduction assay was used to assess H_2O_2 toxicity on SSL and DSL 24, 48, 72 and 96 h after exposure to the first 50- μ M H_2O_2 stress. For this, 50 μ l per well of 5 mg/ml MTT solution (Sigma-Aldrich) were added at each time point assessed to control LUHMES, SSL and DSL cultured in 24-well plates. To promote the formation of formazan crystals, cells were incubated with the MTT solution at 37°C for 3 h after which formazan crystals were solubilized by adding 550 μ l per well of SDS/DMF solution (20% sodium dodecyl sulphate/50% dimethyl formamide, pH 4.7). Plates were incubated at room temperature (RT) for 30 min on a plate shaker to homogenize the samples. Three aliquots of 200 μ l per well were transferred to a 96-well plate for to be read at 595 nm in a PHERAStar microplate reader (BMG Labtech). A medium-only control was used to account for background signal; its absorbance value (arbitrary units [AU]) was subtracted from the AU values of control LUHMES, SSL and DSL samples. Cell viability was expressed as percentage cell viability relative to control.

2.3 | Detection of γ H2AX foci in stressed LUHMES

γ H2AX foci formation was assessed at 6, 24, 48, 72 and 96 h after H_2O_2 treatment in control LUHMES, SSL and DSL. For this, stressed post-mitotic LUHMES cultured in 96-well plates were fixed with 4% paraformaldehyde (PFA) for 10 min, permeabilized in 0.3% Triton-X100 for 3 min and blocked in 3% bovine serum albumin (BSA) for 30 min. For γ H2AX foci detection, cells were incubated with a monoclonal anti- γ H2AX (Ser139) antibody (1:1000, Merck Millipore) for 1 h at RT, followed by incubation with a goat anti-mouse fluorescent secondary antibody (Alexa Fluor 568, 1:1000, ThermoFisher Scientific) for 1 h. Nuclei were stained with Hoechst 33342 (5 μ g/ml bisbenzimidazole in phosphate buffered saline [PBS]). For imaging, 20 fields per well were imaged at 40 \times with the Opera Phenix high content imaging system (Perkin Elmer). Images were analysed using Harmony software, and the percentage of γ H2AX positive nuclei per well and number of γ H2AX foci per cell were determined.

2.4 | CellROX assay

Oxidative stress levels were investigated at 24, 48, 72 and 96 h after H_2O_2 treatment in control LUHMES, SSL and DSL. For this, stressed post-mitotic LUHMES cultured in 96-well plates were incubated with 5- μ M CellROXTM Green Reagent (ThermoFisher Scientific) for 30 min at 37°C. LUHMES were then washed and fixed with 4% PFA for 10 min, permeabilized in 0.3% Triton-X100 for 3 min and blocked in 3% BSA for 30 min. Nuclei were stained with 5 μ g/ml Hoechst 33342 and imaged at 40 \times with the Opera Phenix high content imaging system. Images were analysed using Harmony software, and the intensity of fluorescence was measured.

2.5 | Transcriptome analysis of stressed post-mitotic LUHMES

Microarray analysis was performed on control LUHMES, SSL and DSL to investigate changes in their transcriptome. For this, 96 h after the second 50- μ M H_2O_2 stress, control LUHMES, SSL and DSL cultured in 12-well plates were harvested in Trizol Reagent (ThermoFisher Scientific), and purified RNA was obtained with the Direct-zol RNA MiniPrep extraction protocol (Zymo Research). To assess RNA concentration and integrity, RNA samples were run in an Agilent RNA 6000 Nano Chip (Agilent Technologies INC) (RIN numbers in Table S1).

The 3' IVT Pico Reagent kit (ThermoFisher Scientific) was used to process RNA samples for hybridization to GeneChip Human Genome U133 Plus 2.0 Arrays (ThermoFisher Scientific). Briefly, 10 μ g of RNA/sample were used for double-stranded (ds)-cDNA synthesis, followed by In Vitro Transcription (IVT) to produce complementary RNA (cRNA). Second-cycle ds-cDNA synthesized from cRNA was fragmented and labelled with biotinylated DNA Labelling Reagent and hybridized to the microarray chips, together with hybridization controls (bioB, bioC, bioD and cre) and Oligo B2, for 16 h at 45°C and 60 rpm. Microarray chips were washed and stained in the Fluidics Station 400 and the Gene Chip Operating System (GCOS) and scanned in the GC3000 7G scanner.

2.6 | Validation of microarray data by quantitative real-time polymerase chain reaction

To validate the microarray findings, a number of candidate genes were selected for quantitative polymerase

chain reaction (qPCR) detection and quantification. Extracts collected in Trizol from 96-h control LUHMES, SSL and DSL were used for RNA extraction with the Direct-zol RNA MiniPrep, and Zymo-Spin IIC Columns (Zymo Research) RNA extracts (RIN numbers supplied in Table S1) were processed with qScript cDNA Supermix (Quanta Biosciences) for cDNA synthesis. For qPCR amplification, PrimeTime qPCR assays (Integrated DNA Technologies) were used (Assay IDs: ATR - Hs.PT.56a.39957055; CLSPN - Hs.PT.58.765177; CDC27 - Hs.PT.58.205347; CCNB1 - Hs.PT.56a.39564933; NDUFS3 - Hs.PT.58.24945159; NDUFV3 - Hs.PT.58.24769161; ACTB - Hs.PT.39a.22214847; GAPDH - Hs.PT.39a.22214836). Samples for qPCR experiments had a final volume of 10 μ l per sample and contained 60 ng of cDNA, 500 nM of primers, 250 nM of probe and 2 \times Brilliant III qPCR Master Mix (Agilent Technologies) and were amplified following a two-step thermal profile (10 min at 95°C, then 40 cycles of 30 s at 95°C, 60 s at 60°C and 60 s at 72°C) in a Bio-Rad C1000 Thermal Cycler (Bio-Rad). Expression levels of target genes were normalized to β -actin and GAPDH using the $\Delta\Delta$ Ct calculation.

2.7 | Functional validation: Complex I assay and detection of proliferation markers in stressed post-mitotic LUHMES

Protein lysates from control LUHMES, SSL and DSL were collected at the 96-h time point and processed using the Complex I Enzyme Activity Microplate Assay Kit (Abcam), following the manufacturer's instructions. For this, 50 μ l of protein sample (3.5–4.5 μ g/ μ l) were incubated with 150 μ l of incubation buffer for 3 h at RT in a multiwell plate, after which 200 μ l per well of assay solution were added. Absorbance was detected at 450 nm in a PHERAStar microplate reader every 30 s for 32 min. To obtain the value of oxidized NAD⁺ per min, absorbance values (range, mOD/min) were used to calculate the slope using the MARS Data Analysis Software (BMG Labtech), which was then divided by the extinction coefficient (ϵ) of the dye ($\epsilon = 25.9$) present in the assay solution to convert mOD to mM oxidized NAD⁺/min. Results were reported as mM oxidized NAD⁺/min/ μ g protein, and data were normalized to controls.

Expression of proliferation markers Ki67 and MCM2 for functional validation experiments was assessed by immunocytochemistry. Control LUHMES, SSL and DSL cultured on glass coverslips in 24-well plates were fixed with 4% PFA at the 96-h time point. Detection of Ki67

and Mcm2 was performed by incubating cells with a mouse monoclonal anti-Ki67 antibody (1:50, Leica Microsystems) or a rabbit-polyclonal anti-MCM2 antibody (1:50, Proteintech), together with chicken polyclonal anti- β -III-tubulin (1:1000, Merck Millipore). Cells were then incubated with a goat anti-chicken fluorescent antibody (Alexa Fluor 488, 1:1000) and either a donkey anti-mouse (Alexa Fluor 568, 1:1000) or a donkey anti-rabbit fluorescent antibody (Alexa Fluor 568, 1:1000); nuclei were stained with Hoechst 33342. Proliferating LUHMES were included as positive controls for Ki67 and Mcm2 expression. Cells were imaged with a Nikon ECLIPSE Ni microscope (Nikon Instruments) at 40 \times magnification.

2.8 | Statistical analysis

Data for the cell viability assays, detection of γ H2AX foci, CellROX assay, qPCR validation and Complex I assay, were obtained from at least three biological repeats per condition, with three technical repeats each. The MTT data, the percentage of γ H2AX positive cells and the number of γ H2AX foci per cell were analysed using a repeated measures two-way analysis of variance (ANOVA) with multiple comparisons; the qPCR data were analysed an ordinary one-way ANOVA with multiple comparisons. All data are presented as mean \pm standard error of the mean (SEM), and significance was set at $p \leq 0.05$. All statistical analyses were performed in Prism 7.0c (GraphPad Software).

For the microarray, three replicates per condition were included in the analysis. Quality control assessment was done with Affymetrix Expression Console 1.4.1.46. Expression data were normalized using the Robust Multi-Array Average (RMA) and analysed with the QluCore Omics Explorer software (QluCore). A principal component analysis (PCA) was used to visualize the three different conditions assessed and to identify outliers. A two-group comparison approach was used to detect differentially expressed (DE) transcripts between SSL versus control LUHMES, DSL versus control LUHMES and DSL versus SSL, setting all three analyses at $p \leq 0.05$ and a fold change (FC) ≥ 1.2 . Identification of dysregulated pathways in DSL and SSL was done by uploading the lists of DE transcripts from the three comparisons to IMPaLA (Integrated Molecular Pathway Level Analysis Version 9) (Cavill et al., 2011; Kamburov et al., 2011). The resulting lists of dysregulated pathways are shown in Tables S2–S4.

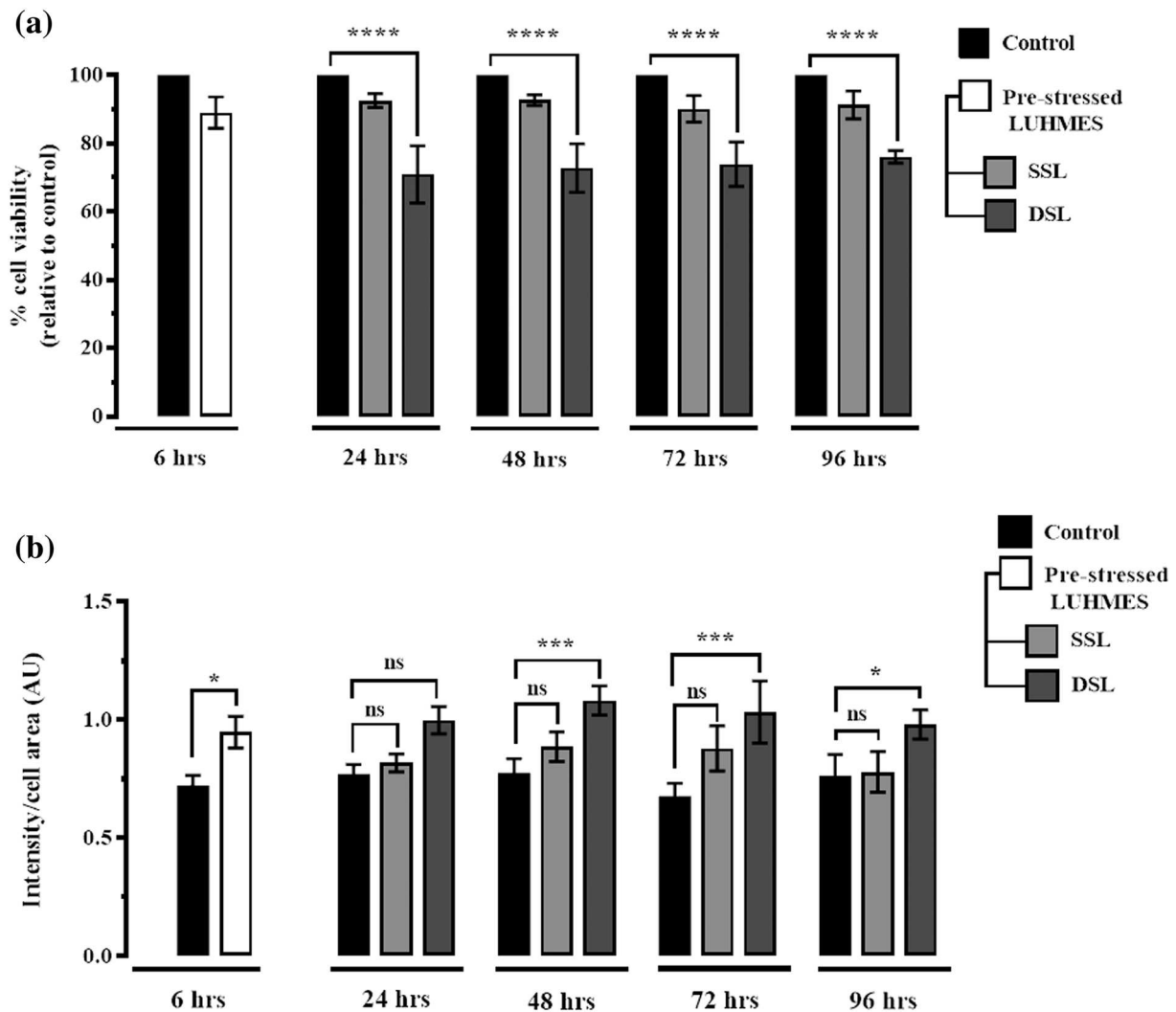


FIGURE 2 Characterization of the double-stress model in post-mitotic LUHMES. (a) Cell viability of LUHMES was investigated using the MTT reduction assay. Exposure of LUHMES to the first 50- μ M H_2O_2 stress caused a non-significant reduction in cell viability of 10% (pre-stressed LUHMES after 6 h). A second dose of 50- μ M H_2O_2 impacted significantly LUHMES' cell viability after 24 h; however, reduction in cell viability was constant over time, with almost 80% of LUHMES being still viable after 96 h. (b) Measurement of oxidative stress detected with the CellROX Green reagent showed increased oxidative stress 6 h after the first H_2O_2 stress. In SSL, this was reduced to non-significant levels comparable with control LUHMES after 24 h, but in DSL, oxidative stress was significantly higher after 48, 72 and 96 h (two-way ANOVA with multiple comparisons; $n = 6$; data represent mean \pm SEM)

3 | RESULTS

3.1 | Exposure to a second dose of 50- μ M H_2O_2 causes oxidative stress and persistent DNA damage in immortalized post-mitotic neurons in vitro

To investigate the effects of persistent DNA damage in neurons, we used the LUHMES cell line, a genetically modified human neuronal cell line that can be kept in culture as neuronal precursor cells and differentiated into post-mitotic neurons as previously described (Scholz et al., 2011). To induce oxidative DNA damage, post-

mitotic LUHMES were stressed with 50- μ M H_2O_2 following a 'single' or 'double stress' protocol (Figure 1). To assess the effect of administering a second stress on post-mitotic LUHMES, cell viability was monitored for 96 h using the MTT assay. LUHMES viability was assessed 6 h after treatment with the first dose of 50- μ M H_2O_2 , which had a non-significant effect on their viability ($89.07\% \pm 4.64\%$, $p = 0.1224$). At this time point, post-mitotic LUHMES were incubated for a second time with 50- μ M H_2O_2 to generate the DSL; cell viability was then analysed 24, 48, 72 and 96 h in SSL, DSL and control LUHMES. A significant reduction of 29.04% (cell viability of $70.96\% \pm 8.39\%$, $p \leq 0.0001$) in cell viability was

detected in DSL when compared with control LUHMES 24 h after the second stress; this significant impact on DSL viability persisted over time (48 h, 27.21% decrease [cell viability of $72.79\% \pm 7.12\%$]; 72 h, 26.08% decrease [cell viability of $73.92\% \pm 6.55\%$]; 96 h, 23.93% decrease [cell viability of $76.07\% \pm 1.81\%$]; all $p \leq 0.0001$). Cell viability was not significantly affected in SSL, which did not receive the second H_2O_2 stress, when compared with control LUHMES at any of the time points assessed (24 h, 92.56 ± 2.03 , $p = 0.3522$; 48 h, 92.73 ± 1.53 , $p = 0.3672$; 72 h, 90.18 ± 3.91 , $p = 0.1769$; 96 h, 91.32 ± 4.08 , $p = 0.2505$) (Figure 2a). Exposure of post-mitotic LUHMES to $50\text{-}\mu\text{M}$ H_2O_2 caused an oxidative environment in DSL (Figure 2b). Six hours after the first stress, oxidative stress was significantly higher in stressed post-mitotic LUHMES compared with controls (0.95 ± 0.06 , $p = 0.0078$), but it reached levels comparable with control LUHMES after 24 h in SSL (24 h, 0.817 ± 0.038 , $p = 0.9588$; 48 h, 0.886 ± 0.063 , $p = 0.1988$; 72 h, 0.879 ± 0.095 , $p = 0.0510$; 96 h, 0.779 ± 0.086 , $p = 0.9325$). In contrast, a second exposure to $50\text{-}\mu\text{M}$ H_2O_2 caused a significant increase in oxidative stress in DSL after 48 h (1.083 ± 0.062 , $p = 0.0007$), 72 h (1.034 ± 0.131 , $p = 0.0004$) and 96 h (0.975 ± 0.062 , $p = 0.0443$).

To determine whether DNA damage had occurred in SSL and DSL, γ H2AX foci formation was tracked over 96 h (Figure 3). γ H2AX+ LUHMES were

detectable 6 h after the first dose of $50\text{-}\mu\text{M}$ H_2O_2 in a significantly higher percentage compared with control LUHMES ($56.71\% \pm 7.06\%$; $p \leq 0.0001$); the mean number of foci per cell at this point was 48.5 ± 7.338 ($p \leq 0.0001$). Twenty-four hours after exposure to a second $50\text{-}\mu\text{M}$ H_2O_2 stress, $32.71\% \pm 1.12\%$ ($p \leq 0.0001$) of DSL and $18.86\% \pm 2.82\%$ ($p = 0.0097$) of the SSL were positive for γ H2AX, and the mean number of foci per cell was of 32 ± 5 ($p \leq 0.0001$) and 2 ± 0.1 ($p = 0.9605$), respectively. Although the mean percentage of γ H2AX+ cells in the DSL model decreased over time, it remained significantly higher than controls (48 h, $32.11\% \pm 2.67\%$, $p \leq 0.0001$; 72 h, $31.73\% \pm 5.18\%$, $p \leq 0.0001$; 96 h, $19.20\% \pm 2.24\%$, $p \leq 0.0001$). The number of foci per cell was also significantly higher in DSL (48 h, 23 ± 2 , $p = 0.9946$; 72 h, 26 ± 7 , $p = 0.9813$; 96 h, 17 ± 2 , $p = 0.9946$), which confirmed that a small yet significant percentage of γ H2AX+ LUHMES were still detectable in DSL even 96 h after the second H_2O_2 dose. The same did not occur with SSL, where the percentage of γ H2AX+ LUHMES decreased significantly after 48 h and were similar to control LUHMES after 72 and 96 h (48 h, 14.86 ± 2.33 , $p = 0.0101$; 72 h, 6.43 ± 0.90 , $p = 0.6607$; 96 h, 8.08 ± 0.72 , $p = 0.4644$); the number of foci per cell also decreased to non-significant levels after 96 h in SSL (48 h, 2 ± 0.27 , $p = 0.9804$; 72 h, 3 ± 0.47 , $p = 0.8228$; 96 h, 2 ± 0.21 , $p = 0.9984$).

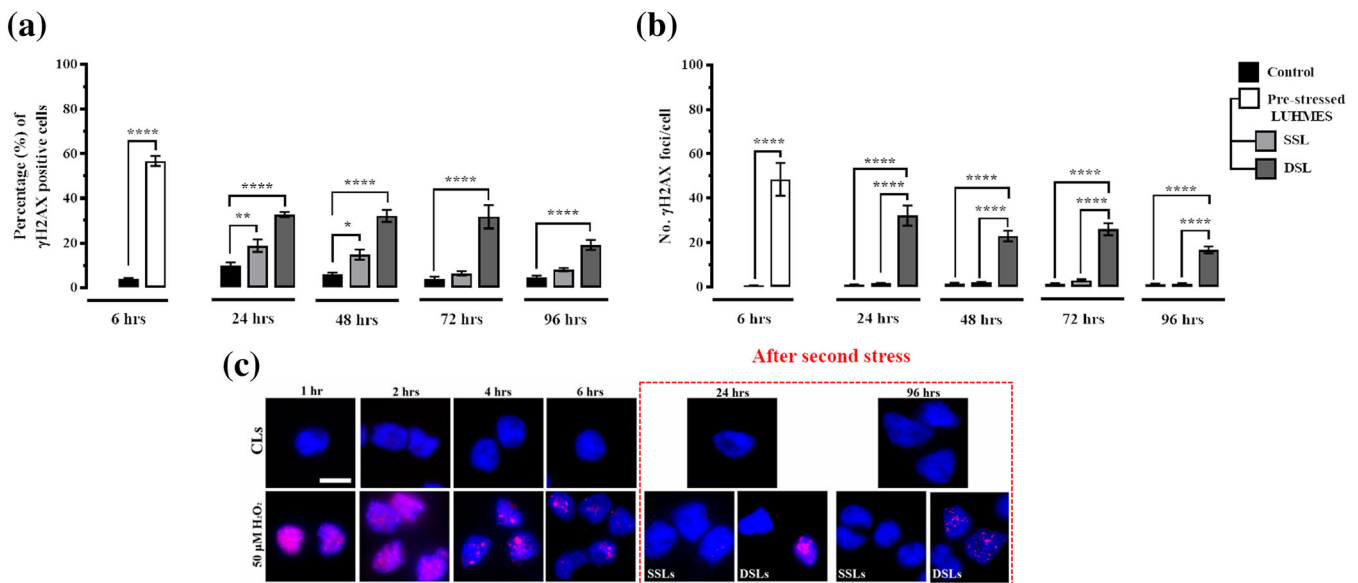


FIGURE 3 Detection of γ H2AX foci formation in the double-stress model in post-mitotic LUHMES. (a) Quantification of γ H2AX positive cells over time indicated that 20% of the quantified nuclei were positive γ H2AX in the DSL after 96 h (one-way ANOVA with multiple comparisons; $n = 3$; data represent mean \pm SEM). (b) Quantification of the number of γ H2AX foci per cell also indicated a significantly higher number in DSL, compared with SSL and control LUHMES, although this number of foci per cell decreased with time. (c) Detection of γ H2AX foci by immunocytochemistry confirmed that one dose of $50\text{-}\mu\text{M}$ H_2O_2 caused DSBs formation that were detected 1 h after stress (pre-stressed LUHMES) and resolved after 24 h (SSL), whereas a second $50\text{-}\mu\text{M}$ H_2O_2 induced DSBs formation that were detected even after 96 h (DSL). Scale bar represents 10 μm

3.2 | Persistent oxidative DNA damage induces gene expression changes in ATR-dependent DDR and APC/C cell cycle regulatory complex pathways as well as in mitochondrial function

Microarray gene expression analysis was used to assess the transcriptomic changes in SSL and DSL 96 h after the second dose of H₂O₂. PCA showed a clear segregation between control, SSL and DSL, with the three replicates for each condition grouping together (Figure 4a). Challenging LUHMES with H₂O₂ caused a significant change in their transcriptome (Figure 4b); moreover, a second H₂O₂ stress induced a different gene expression pattern in DSL to the one observed in SSL when compared with control LUHMES (Figure 4c,d). The two-group comparison analyses revealed 1285 DE transcripts in DSL compared with control LUHMES (695, up-regulated; 590, down-regulated) and 1607 DE transcripts when

compared with SSL (649, up-regulated; 958 down-regulated). Comparison of SSL against control LUHMES revealed a total of 450 DE transcripts, with 276 being up-regulated and 174 being down-regulated.

The lists of dysregulated transcripts were transferred to IMPaLA to conduct enrichment analysis of the three sets of data. Analysis of DSL transcriptome compared with control LUHMES suggested significant changes in cell cycle signalling, DDR and repair and mitochondrial function (Tables 1 and S2). Dysregulation of cell cycle mechanisms was mainly linked to the anaphase promoting (APC/C) cell cycle regulatory complex (Pathways: APC/C:Cdc20 mediated degradation of mitotic proteins, Activation of APC/C and APC/C:Cdc20 mediated degradation of mitotic proteins, APC/C:Cdc20 mediated degradation of Cyclin B, Regulation of APC/C activators between G1/S and early anaphase), and DDR and repair pathways pointed at ATR-dependent DDR (Pathways: Homology directed repair [HDR] through homologous

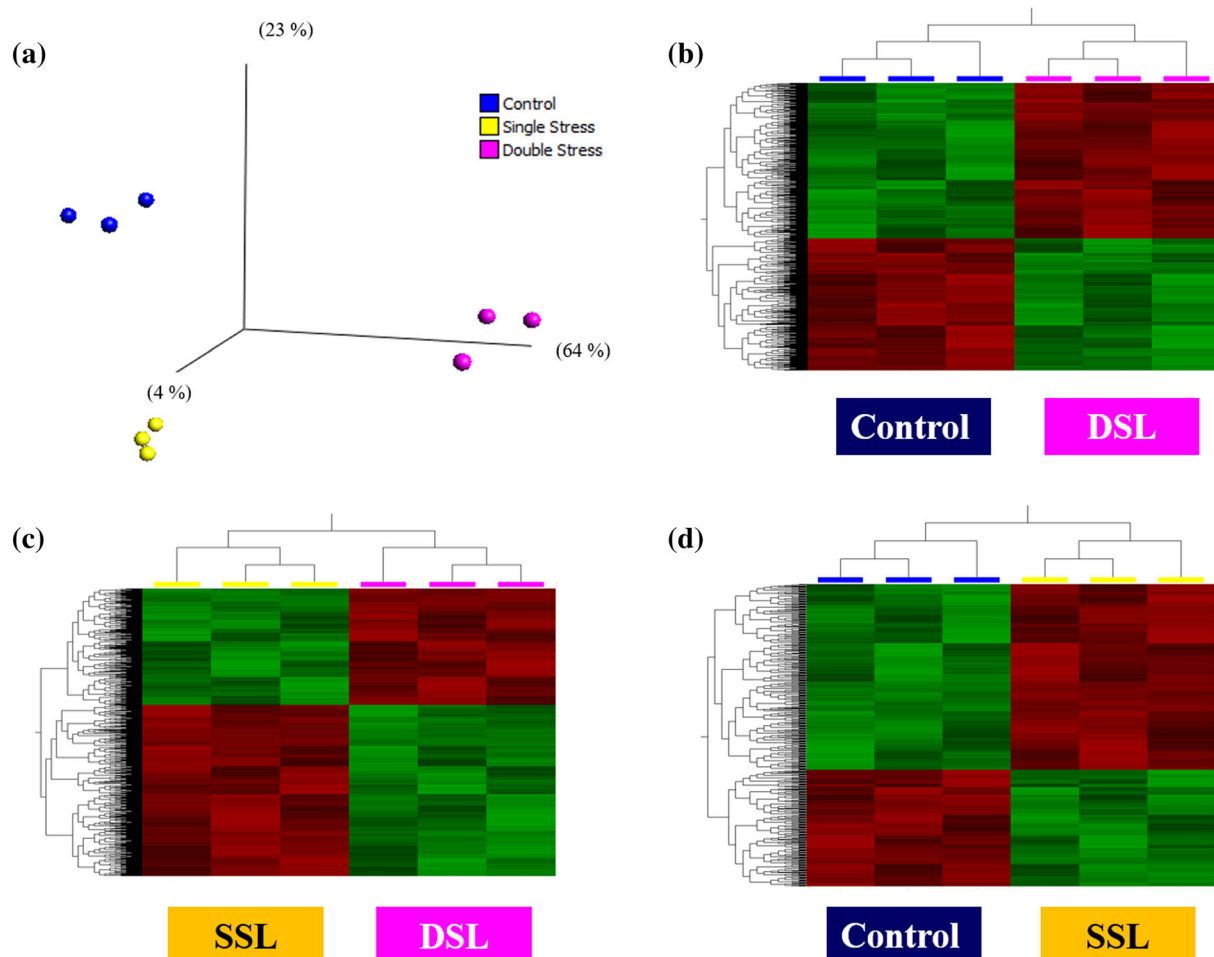


FIGURE 4 Gene expression analysis of 96-h SSL and DSL. (a) Principal component analysis of microarray data showing a clear separation between control LUHMES (blue), SSL (yellow) and DSL (pink) using a multigroup analysis. Two-way comparisons were also performed to identify changes in gene expression in DSL. Heatmaps showing up-regulated (green) and down-regulated (red) gene expression (FC \geq 1.2, $p \geq$ 0.05) in the SSL versus control LUHMES (b), DSL versus control LUHMES (c) and DSL versus SSL (d)

TABLE 1 IMPaLA pathway analysis of the total number of differentially expressed transcripts in DSL compared with control LUHMES: Top dysregulated pathways

Pathway name	Pathway source	Overlapping genes	p-value
Gene expression	Reactome	103	3.81E-05
Generic transcription pathway	Reactome	59	3.86E-06
HDR through homologous recombination or single strand annealing (SSA)	Reactome	15	0.000343
Homology directed repair	Reactome	15	0.00055
SUMO E3 ligases SUMOylate target proteins	Reactome	13	0.00115
DNA double-strand break repair	Reactome	16	0.00123
Signalling by TGF-beta family members	Reactome	11	0.00172
Antigen processing: Ubiquitination and proteasome degradation	Reactome	21	0.00212
Neural crest differentiation	Wikipathways	11	0.00233
E-cadherin signalling in the nascent adherens junction	PID	6	0.00319
HDR through single strand annealing (SSA)	Reactome	6	0.00383
Hippo signalling pathway—multiple species— <i>Homo sapiens</i> (human)	KEGG	5	0.00421
Cardiac progenitor differentiation	Wikipathways	7	0.00478
Toxicity of botulinum toxin type A (BoNT/A)	Reactome	2	0.00492
Teniposide action pathway	SMPDB	2	0.00492
Teniposide metabolism pathway	SMPDB	2	0.00492
Post-translational regulation of adherens junction stability and disassembly	PID	7	0.00511
Regulation of TP53 activity	Reactome	14	0.00621
APC/C:Cdc20 mediated degradation of mitotic proteins	Reactome	5	0.00769
VEGF and VEGFR signalling network	PID	3	0.00778
LICAM interactions	Reactome	10	0.00793
p53 signalling pathway—<i>H. sapiens</i> (human)	KEGG	8	0.00851
Syndecan-4-mediated signalling events	PID	5	0.00876
Activation of APC/C and APC/C:Cdc20 mediated degradation of mitotic proteins	Reactome	5	0.00876
Neovascularization processes	Wikipathways	4	0.00924
Antagonism of activin by follistatin	Reactome	2	0.00958
Toxicity of botulinum toxin type D (BoNT/D)	Reactome	2	0.00958
Toxicity of botulinum toxin type F (BoNT/F)	Reactome	2	0.00958
Neurophilin interactions with VEGF and VEGFR	Reactome	2	0.00958
E-cadherin signalling in keratinocytes	PID	4	0.00967
Transcriptional misregulation in cancer— <i>H. sapiens</i> (human)	KEGG	14	0.0114

(Continues)

TABLE 1 (Continued)

Pathway name	Pathway source	Overlapping genes	p-value
APC/C:Cdc20 mediated degradation of Cyclin B	Reactome	4	0.0114
Mycophenolic acid pathway_pharmacokinetics/ pharmacodynamics	PharmGKB	3	0.0115
ATR signalling pathway	PID	5	0.0118
Regulation of APC/C activators between G1/S and early anaphase	Reactome	5	0.0119
Circadian clock	Reactome	5	0.0128
Cell cycle checkpoints	Reactome	18	0.0129
The citric acid (TCA) cycle and respiratory electron transport	Reactome	6	0.0133
Signalling pathways regulating pluripotency of stem cells— <i>H. sapiens</i> (human)	KEGG	12	0.0133

TABLE 2 Transcripts involved in DDR and repair pathways that are dysregulated in DSL

DDR and repair				
Gene symbol	Gene title	p-value	Up/down-regulated	Fold change
Pathways: ATR signalling				
<i>RPA1</i>	Replication protein A1	0.0210	Down	0.7533
<i>TIPIN</i>	TIMELESS interacting protein	0.0073	Down	0.7827
<i>ATR</i>	ATR serine/threonine kinase	0.0169	Up	1.2074
<i>CLSPN</i>	Claspin	0.0055	Up	1.2351
<i>PPP2R2B</i>	Protein phosphatase 2, regulatory subunit B, beta	0.0157	Up	1.4043
Pathways: Homology directed repair (HDR) and HDR through homologous recombination or single strand annealing (SSA), Homology directed repair, DNA double-strand break repair and HDR though single strand annealing				
<i>HIST1H2BM</i>	Histone cluster 1, H2bm	0.0407	Down	0.5931
<i>TOP3A</i>	Topoisomerase (DNA) III alpha	0.0380	Down	0.7254
<i>ERCC1</i>	Excision repair cross-complementation group 1	0.0152	Down	0.7454
<i>RPA1</i>	Replication protein A1	0.0210	Down	0.7533
<i>TIPIN</i>	TIMELESS interacting protein	0.0073	Down	0.7827
<i>RPS27A</i>	Ribosomal protein S27a	0.0088	Down	0.7917
<i>RNF4</i>	Ring finger protein 4	0.0269	Down	0.7985
<i>RHNO1</i>	RAD9-HUS1-RAD1 interacting nuclear orphan 1	0.0241	Down	0.8024
<i>RAD52</i>	RAD52 homologue, DNA repair protein	0.0247	Down	0.8164
<i>HIST1H4C</i>	Histone cluster 1, H4c	0.0316	Down	0.8201
<i>ATR</i>	ATR serine/threonine kinase	0.0169	Up	1.2074
<i>HIST1H4A</i>	Histone cluster 1, H4a	0.0308	Up	1.2286
<i>CLSPN</i>	Claspin	0.0055	Up	1.2351
<i>RIF1</i>	Replication timing regulatory factor 1	0.0346	Up	1.2396
<i>SPIDR</i>	Scaffolding protein involved in DNA repair	0.0456	Up	1.3261
<i>RAD51B</i>	RAD51 paralog B	0.0338	Up	1.4945

recombination or single strand annealing [SSA], Homology directed repair, DNA double-strand break repair, HDR through SSA and ATR signalling pathway); we also

identified changes in mitochondrial function, specifically in the respiratory electron transport chain pathway. There was no overlap between dysregulated pathways

identified in DSL with the dysregulated pathways identified in SSL when compared with control LUHMES (Table S3); however, when looking at the comparison between DSL versus SSL, cell cycle regulatory pathways (Pathways: Cell cycle, APC/C:Cdc20 mediated degradation of Securin, Cell cycle_mitotic), as well as DDR (Pathways: DNA damage response, Activation of ATR in response to replication stress) and mitochondrial electron transport chain were also significantly altered (Pathways: The citric acid [TCA] cycle and respiratory electron transport) (Table S4). The transcripts involved in the dysregulated pathways identified by IMPaLA in the DSL model are listed in Tables 2 and 3. qPCR validation of these results was conducted in independent DSL, SSL and control LUHMES by assessing the levels of the top most DE transcripts or the transcripts that encode for main proteins in these pathways (Tables 2 and 3, transcripts highlighted in bold type). *NDUFV3* and *NDUFS3* both encode for mitochondrial Complex I proteins and were chosen for validation of altered mitochondrial function in DSL; altered DDR and cell cycle changes in neurons in response to DNA damage have been reported previously (Kruman et al., 2004; Tomashevski et al., 2010), but we focused our analysis on the role of

ATR and APC/C^{Cdc20} in the DSL model and chose *ATR*, *CLSPN*, *CCNB1* and *CDC27* to validate these changes.

3.3 | qPCR and functional validation confirmed mitochondrial Complex I hyperactivation in immortalized post-mitotic neurons exposed to persistent oxidative DNA damage

Microarray results suggested dysregulated expression of transcripts linked to mitochondrial Complex I, ATR-dependent DDR and APC/C:Cdc20 complex. To confirm these results, we analysed their expression levels by qPCR in independent control LUHMES, SSL and DSL. Assessment of *NDUFS3* (array: FC = 0.779, $p = 0.036$) expression identified a significant decrease in the levels of this transcript in both SSL ($p < 0.01$) and DSL ($p < 0.05$) (Figure 5a), which validated the microarray data in DSL but suggested down-regulation in SSL that was not detected by the microarray. Changes in *NDUFV3* (array: FC = 0.753, $p = 0.005$) expression in DSL did not reach significance but showed the same directional change that was observed in the microarray and confirmed down-

TABLE 3 Transcripts involved in cell cycle regulatory pathways and mitochondrial function that are dysregulated in DSL

Cell cycle regulation				
Pathways: APC/C:Cdc20 mediated degradation of mitotic proteins, APC/C:Cdc20 mediated degradation of mitotic proteins, APC/C:Cdc20 mediated degradation of Cyclin B and Regulation of APC/C activators between G1/S and early anaphase				
Gene symbol	Gene title	p-value	Up/down-regulated	Fold change
<i>ANAPC10</i>	Anaphase promoting complex subunit 10	0.0283	Down	0.7097
<i>RPS27A</i>	Ribosomal protein S27a	0.0088	Down	0.7917
<i>CCNB1</i>	Cyclin B1	0.0404	Down	0.8273
<i>CDC27</i>	Cell division cycle 27	0.0420	Down	0.8285
<i>MAD2L1</i>	MAD2 mitotic arrest deficient-like 1 (yeast)	0.0315	Up	1.3502
Mitochondrial function				
Pathways: The citric acid (TCA) cycle and respiratory electron transport				
Gene symbol	Gene title	p-value	Up/down-regulated	Fold change
<i>NDUFV3</i>	NADH dehydrogenase (ubiquinone) flavoprotein 3, 10 kDa	0.0053	Down	0.7535
<i>NDUFS3</i>	NADH dehydrogenase (ubiquinone) Fe-S protein 3, 30 kDa (NADH-coenzyme Q reductase)/protein tyrosine phosphatase, mitochondrial 1	0.0363	Down	0.7793
<i>UQCRCQ</i>	Ubiquinol-cytochrome c reductase Complex III subunit VII	0.0428	Down	0.8054
<i>IDH3G</i>	Isocitrate dehydrogenase 3 (NAD ⁺) gamma	0.0486	Down	0.8129
<i>NNT</i>	Nicotinamide nucleotide transhydrogenase	0.0187	Down	0.8269
<i>ADHFE1</i>	Alcohol dehydrogenase, iron containing 1	0.0255	Up	1.2210
<i>COQ10B</i>	Coenzyme Q10B	0.0432	Up	1.3381

regulation of this transcript (Figure 5b). To investigate whether altered expression of *NDUFV3* and *NDUFS3* had an effect on mitochondrial Complex I activity in DSL, we measured NADH oxidation to NAD⁺, a mechanism dependent on Complex I activity. Functional assessment revealed a significant increase of 2.75 ± 0.24 fold in Complex I activity in DSL ($p = 0.002$) compared with control LUHMES, whereas there was no significant change in Complex I activity of SSL (1.24 ± 0.44 fold, $p = 0.6829$) (Figure 5c).

Dysregulation of APC/C complex genes *CCNB1* (array: FC = 0.827, $p = 0.040$) and *CDC27* (array: FC = 0.828, $p = 0.041$) was not significant in DSL when measured by qPCR (*CDC27*, $p = 0.3900$; *CCNB1*, $p = 0.4329$) (Figure 6a,b). qPCR analysis of *CLSPN* levels (array: FC = 1.23, $p = 0.005$) showed a trend towards increased expression, although this did not reach significance (SSL, $p = 0.4329$; DSL, $p = 0.9912$) (Figure 6c), whereas *ATR* (array: FC = 1.207, $p = 0.016$) in DSL showed a directional change towards up-regulation as seen in the microarray, which did not reach significance ($p = 0.1547$) (Figure 5d). On the other hand, *ATR* expression was significantly up-regulated in SSL ($p = 0.0175$) (Figure 5d). We investigated cell cycle re-entry in SSL and DSL to assess whether this was related to the identification of cell cycle pathways dysregulation at the transcriptomic level; however, expression of cell proliferation markers Ki67 and MCM2 were absent in DSL when assessed by immunocytochemistry (Figure 5e).

4 | DISCUSSION

Oxidative DNA damage occurs in the ageing brain and is a feature of neurodegeneration (Bogdanov et al., 2000;

Murata et al., 2008; Silva et al., 2014; Simpson et al., 2015). Unrepaired persistent DNA damage and altered DDR could promote neuronal dysfunction and lead to neuronal death in these pathologies (Adamec et al., 1999; Bender et al., 2006; Jacobsen et al., 2004; Kraysberg et al., 2006; Mullaart et al., 1990). Here, we report an in vitro model of persistent oxidative DNA damage in the LUHMES cell line and investigate their transcriptomic signature. We show that persistent oxidative DNA damage causes gene expression and cell pathway changes relevant to cell cycle regulation, DDR and mitochondrial Complex I function. Moreover, our study confirms hyperactivation of mitochondrial Complex I, which could be partly contributing to the sustained DNA damage and DDR that is observed in our model and in neurons in neurodegenerative pathologies.

Although ROS have a physiological role in neurons in signal transduction, their accumulation is detrimental and causes damage to proteins, lipids and nucleic acids. We investigated the impact of oxidative DNA damage in the transcriptome of post-mitotic LUHMES. Exposure to a single dose of a sublethal concentration of H₂O₂ promoted an oxidative environment and caused oxidative DNA damage in the form of DSBs that were detected through γ H2AX foci formation very early after treatment. γ H2AX is widely used as a marker of DSBs, as the number of phosphorylated H2AX molecules correlates with the quantity of DNA damage (Paull et al., 2000; Rogakou et al., 1998). Phosphorylation of histone H2AX at Serine-139 is an essential step of the DDR cascade, stimulating recruitment of ATM to the site of the damage, which is then followed by either activation of repair mechanisms or induction of cell death (Kinner et al., 2008; Rogakou et al., 1998). In post-mitotic LUHMES, increased oxidative stress and γ H2AX foci were still visible in the nuclei

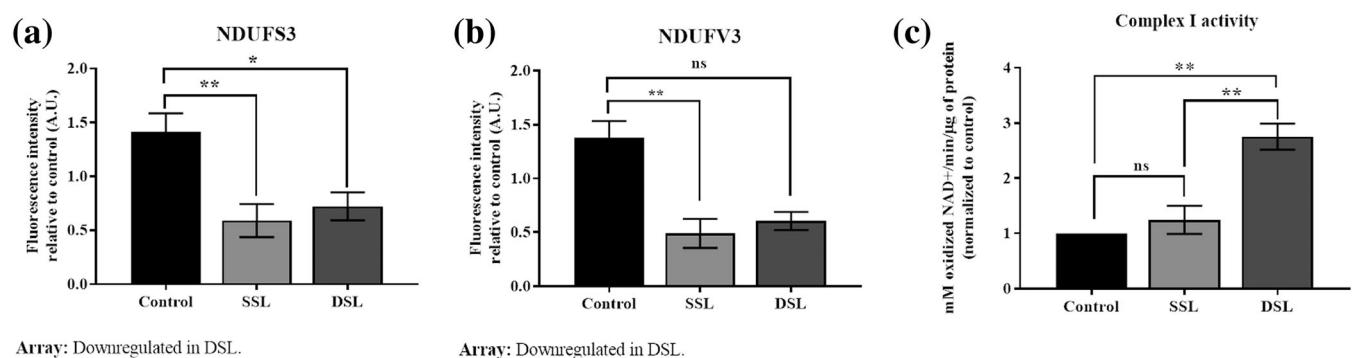


FIGURE 5 qPCR and functional validation of mitochondrial Complex I differentially expressed transcripts in 96-h DSL. (a) qPCR validation of *NDUFS3* confirmed down-regulation in 96-h DSL as detected in the microarray; qPCR validation also revealed down-regulation of *NDUFS3* in SSL, but this was not detected in the microarray. (b) *NDUFV3* down-regulation detected in the microarray only reached significance in SSL but showed the same directional change in DSL. (c) Mitochondrial Complex I function was assessed in 96-h control LUHMES, SSL and DSL by measuring NADH-dependent Complex I activity. A significant hyperactivity in Complex I was seen in DSL, reflected in a significant increase in oxidized NAD⁺/min/μg (one-way ANOVA with multiple comparisons; $n = 3$; data represent means \pm SEM)

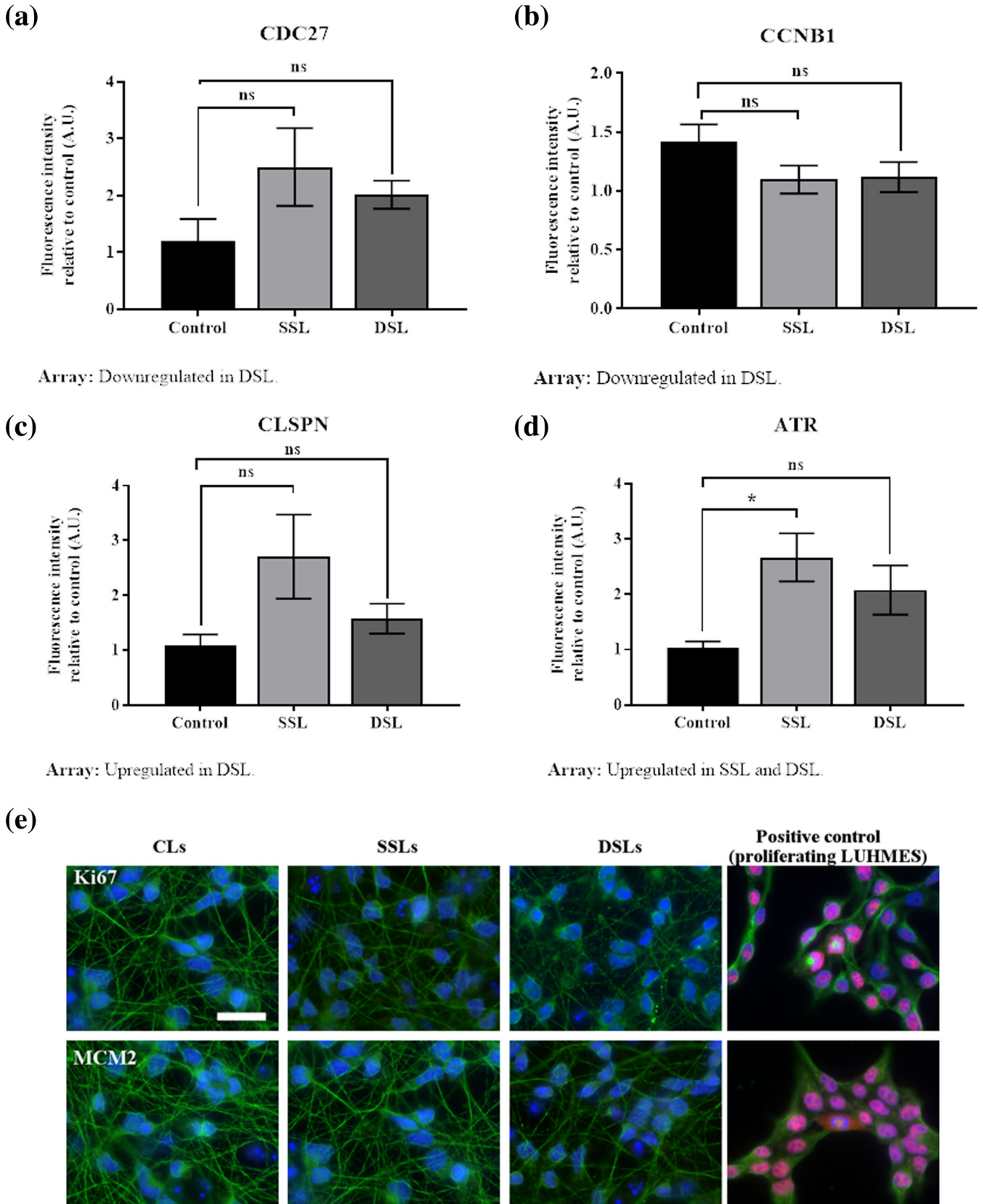


FIGURE 6 Legend on next page.

FIGURE 6 qPCR validation of ATR-dependent DDR and cell cycle dysregulated transcripts in 96-h DSL and expression of proliferation markers. (a–d) Dysregulated transcripts involved in ATR-dependent DDR signalling were measured by qPCR. *CDC27* and *CCNB1* were significantly down-regulated in the microarray data. The same directional change was found with qPCR for *CCNB1* (a, b), although this did not reach significance. Microarray analysis showed up-regulation of *CLSPN* and *ATR* transcripts, and this was not confirmed by qPCR validation (c, d) (one-way ANOVA with multiple comparisons; $n = 4$; data represent means \pm SEM). (e) No indication of cell cycle reactivation was seen in DSL. Expression of proliferation markers Ki67 (red) and MCM2 (red) colocalized with the nucleus (blue) in proliferating LUHMES but not in differentiated control LUHMES, DSL or SSL (β -III-tubulin is shown in green). Scale bar represents 20 μ m

6 h after the first H_2O_2 dose, but these were fully repaired after 24 h without causing a significant reduction in the percentage of viable cells, suggesting that most damage was repaired rather than inducing cell death. By exposing LUHMES to a second dose of H_2O_2 before previously induced DNA damage was completely repaired, we caused persistent formation of DSBs that were detectable for up to 96 h; at this stage, even though a tendency for increased oxidative stress was detected, it was not statistically significant. Apart from the formation of γ H2AX foci, the identification of significant p53 signalling-associated transcripts in our microarray study also correlates with the activation of repair and cell death mechanisms in the DSL model. More detailed quantification confirmed a significantly higher number of γ H2AX foci/neuron in DSL after 96 h; however, it did not reveal an increase of these foci over time. This suggests that although the second exposure to H_2O_2 causes a persistent formation of DSBs, there is no evidence of oxidative stress having an effect on DSBs repair capacity in our model and our approach does not allow determination of whether the foci that were detected 96 h after treatment were unresolved foci from the first stress or whether they were a new consequence of the second H_2O_2 dose. In the context of our model, formation of γ H2AX foci was directly related to the oxidative stress that post-mitotic LUHMES were exposed to. However, it is important to note that DSBs formation in neurons also occurs at physiological levels, as a result of network activity (Suberbielle et al., 2013). Interestingly, baseline levels of DSBs formation were altered in a transgenic mouse model of AD and hyperactivity in networks involved in memory and learning promoted severe and prolonged DSBs, suggesting that aberrant neural activity can also contribute towards accumulation of DNA damage in neurodegeneration (Suberbielle et al., 2013).

Acute and persistent oxidative DNA damage have differing effects on the gene expression profile of post-mitotic LUHMES. While dysregulation of pathways linked to cellular responses to stress, senescence, tumour necrosis factor (TNF)-signalling pathway and cellular responses to hypoxia were observed in SSL 96 h after stress (Table S4), pathways suggesting altered cell cycle signalling, ATR-dependent DDR and mitochondrial

function were a feature of DSL at the same time point. Our data from SSL is comparable with previous reports on transcriptomic changes in rat hippocampal neurons exposed to oxygen glucose deprivation (OGD), suggesting that acute exposure of LUHMES to H_2O_2 resembles the response seen in acute ischaemic injury (Shi et al., 2017). In contrast, changes seen in DSL, together with the persistent presence of DNA damage foci, point towards gene expression changes caused by genomic instability, a chronically active DDR and mitochondrial dysfunction that characterize age-related neuronal decline (Fakouri et al., 2019).

Dysregulation of *NDUFS3* and *NDUFV3* transcripts, which encode for mitochondrial Complex I subunits NADH dehydrogenase (ubiquinone) Fe-S protein 3 and NADH dehydrogenase (ubiquinone) flavoprotein 3, respectively, occurred in the persistent DNA damage model. As part of the mitochondrial electron transport chain, Complex I uses oxidative phosphorylation to generate ATP from electrons generated through glycolysis, fatty acid oxidation and the tricarboxylic acid (TCA) cycle (Sazanov, 2015). Altered expression of Complex I transcripts suggested impaired activity in the DSL model, but functional assessment revealed hyperactivity of Complex I, contrary to what was expected. Complex I hyperactivity could precede Complex I deficiency reported in neurodegenerative disorders, such as PD (Gatt et al., 2016; Keeney et al., 2006); however, its role in disease is still not understood, and further studies are required to identify whether it could be a therapeutic target. Complex I dysfunction in our model could be linked to a compensatory mechanism occurring in different ways. The hyperactivity detected could be a response to down-regulation of Complex I transcripts in an attempt to maintain neuronal energy levels, eventually causing ROS formation and contributing to oxidative stress. Whether Complex I hyperactivation would be enough to sustain energy levels in DSL and for how long this mechanism could persist is not known. On the other hand, Complex I is the main site of ROS generation and is present in lower levels in the mitochondria compared with other complexes (Schägger & Pfeiffer, 2001), making it more vulnerable to oxidative stress. In this scenario and as a result of this particular vulnerability, Complex I

function could have been affected by exposure to H₂O₂, causing hyperactivity and resulting in down-regulation of Complex I transcripts to counteract this aberrant activity.

Microarray analysis also identified dysregulation of DDR and repair and cell cycle regulatory pathways that are associated with ATR signalling and the APC/C complex. The DDR and cell cycle are closely interlinked. However, these mechanisms are executed differently in post-mitotic neurons compared with cycling cells. Differentiated neurons normally rest in G₀ phase; when exposed to genotoxic stress, DNA damage induces cell cycle re-activation as part of the DDR and DNA repair mechanisms (Kruman et al., 2004; Schwartz et al., 2007; Tomashevski et al., 2010). DSBs caused by oxidative stress, for example, mainly promote activation of the ATM pathway in neurons (Alvira et al., 2007; Kruman et al., 2004; Otsuka et al., 2004); as part of this response, neurons exit G₀ and initiate G₁ phase of their cell cycle, at which point the non-homologous end-joining (NHEJ) repair machinery is recruited (Schwartz et al., 2007). Phosphorylation of H2AX is mainly conducted by ATM (Burma et al., 2001), which would suggest that detection of γ H2AX in our model is mainly linked to activation of ATM-dependent DDR in response to H₂O₂; however, we did not identify transcriptomic changes linked to this pathway in the microarray analysis. It is possible that the ATM-dependent DDR occurs in the first hours after exposure to the first and second doses of H₂O₂, explaining why these changes were not detected at the 96-h time point. Moreover, even though ATM transcription has been shown to be affected by genotoxic stress (Moiola et al., 2012), its activation and of ATM-dependent downstream proteins are regulated by post-translational modifications (Guo et al., 2010), meaning that induction of ATM-dependent DDR in LUHMES exposed to H₂O₂ would have not been detected by our approach.

Contrary to ATM-dependent DDR, the ATR pathway is less understood in neurons, but it is known that it phosphorylates H2AX in response to replication stress in other cell types (Ward & Chen, 2001). ATR-dependent DDR signalling is triggered in response to replication stress during S-phase, which entails activation of G₂/M cell cycle checkpoints through Chk1 phosphorylation with the help of claspin, and induction of repair through homologous recombination (HR) (Liu et al., 2006; Petermann & Caldecott, 2006). Under sublethal conditions, damaged neurons progress from G₀ to G₁ during cell cycle re-activation; when the damage cannot be repaired, neurons transition from G₁ to S-phase, causing aberrant DNA synthesis and apoptosis (Schwartz et al., 2007). The APC/C complex, a multimeric E3 ubiquitin ligase that participates in G₂ DNA damage-induced cell cycle arrest, is active during G₁ to prevent

early S-phase entry and can be reactivated during S/G₂ in response to DNA damage (Bassermann et al., 2008; Sudo et al., 2001). Alteration of both ATR and APC/C-related transcripts in DSL could point to S-phase progression and an attempt to induce DNA synthesis, causing replication stress and activation of ATR-dependent DDR; however, further studies focused on tracking the activation of these pathways in the DSL model are necessary to confirm whether this is occurring and if it is a consequence of persistent DNA damage. Dysregulation in APC/C complex genes could also relate to other mechanisms not linked to cell cycle or DDR, such as neuronal metabolism (Herrero-Mendez et al., 2009) and axonal growth (Konishi, 2004).

One of the limitations of this study is that transcriptomic changes were investigated 96 h after H₂O₂; following up gene expression changes in SSL and DSL in the immediate hours after oxidative stress would inform in more detail of the impact that it has on the neuronal transcriptome. Moreover, assessing H₂O₂ exposure using a different model, such as directly reprogrammed patient-derived neurons (iNeurons) from donors of different ages would help to elucidate what occurs when ageing neurons are exposed to oxidative stress and persistent DNA damage. As shown previously, iNeurons retain their ageing signature (Mertens et al., 2015; Tang et al., 2017), and investigating their response to oxidative stress at the transcriptomic level could identify pathways that are particularly vulnerable to this type of genotoxic stress and that could promote alteration of several mechanisms, such as proteostasis, neuronal activity and inflammation. Also, further studies are necessary to identify the role that ATR and the APC/C complex play in the context of neuronal DNA damage not only at the transcriptomic level; for instance, tracking the activation of these pathways at the protein level could help characterize their function in damaged neurons. Alteration of mitochondrial Complex I genes and function in DSL suggests sensitivity of this complex to persistent oxidative stress. The use of molecules that have been shown to impact Complex I, such as ursodeoxycholic acid (UDCA) (Mortiboys et al., 2013), mitochondrial-division inhibitor 1 (Mdivi-1) (Manczak et al., 2019), AICAR (Golubitzky et al., 2011) or KH176 (Frambach et al., 2020), could help investigate if boosting mitochondrial Complex I has an effect on oxidative stress levels and oxidative DNA damage in DSL.

5 | CONCLUSIONS

The results of this study demonstrate that acute and persistent oxidative DNA damage have different effects on

the transcriptomic profile of immortalized post-mitotic neurons. The transcripts that were significantly affected by persistent oxidative DNA damage were linked to mitochondrial Complex I function, cell cycle regulation and ATR-dependent DDR. Evaluation of Complex I function revealed hyperactivity, suggesting that a persistent oxidative environment has a detrimental effect on mitochondria in our model. Dysregulation in the expression of ATR signalling genes as well as of APC/C-related transcripts could reflect cell cycle re-entry and replication stress in post-mitotic LUHMES; however, the exact way in which these gene expression changes translate to alteration of the neuronal cell cycle remains to be determined. The changes seen in the persistent DNA damage model described in this study could contribute to the maintenance of an oxidative environment in the ageing brain and could be occurring very early in neurodegeneration; understanding these changes will help in the identification of therapeutic targets for neurodegenerative diseases.

ACKNOWLEDGEMENTS

IV-V was supported by Consejo Nacional de Ciencia y Tecnología (CONACyT), Mexico, Fellow No. 217532, and by a grant from Alzheimer's Research UK (PG2019A-003) to SBW, PRH and JES. SBW, PRH and JES also received support from the UK Medical Research Council (MR/J004308/1).

CONFLICT OF INTEREST

The authors declare no conflict of interest. The funders had no role in the design of the study; in the collection, analyses or interpretation of data; in the writing of the manuscript; or in the decision to publish the results.

AUTHOR CONTRIBUTIONS

The study was conceived by SBW. IV-V planned and carried out the experiments, performed the analysis and wrote the first draft of the paper. SBW and JES supervised the project. PH supervised the molecular and array work, and HM supervised the mitochondrial studies and interpretation. All of the authors contributed to the interpretation of findings and the final version of the paper.

PEER REVIEW


The peer review history for this article is available at <https://publons.com/publon/10.1111/ejn.15466>.

DATA AVAILABILITY STATEMENT

The microarray dataset generated for this study is freely available at Gene Expression Omnibus, accession number GSE160841. All other datasets are available from the corresponding author upon reasonable request.

ORCID


Irina Vazquez-Villasenor  <https://orcid.org/0000-0002-1668-7797>

Claire J. Garwood  <https://orcid.org/0000-0001-8611-177X>

Julie E. Simpson  <https://orcid.org/0000-0002-3753-4271>

Paul R. Heath  <https://orcid.org/0000-0002-8385-1438>

Heather Mortiboys  <https://orcid.org/0000-0001-6439-0579>

Stephen B. Wharton  <https://orcid.org/0000-0003-2785-333X>

REFERENCES

- Adamec, E., Vonsattel, J. P., & Nixon, R. A. (1999). DNA strand breaks in Alzheimer's disease. *Brain Research*, *849*, 67–77. [https://doi.org/10.1016/S0006-8993\(99\)02004-1](https://doi.org/10.1016/S0006-8993(99)02004-1)
- Ajikumar, A., Long, M. B., Heath, P. R., Wharton, S. B., Ince, P. G., Ridger, V. C., & Simpson, J. E. (2019). Neutrophil-derived microvesicle induced dysfunction of brain microvascular endothelial cells in vitro. *International Journal of Molecular Sciences*, *20*(20), 5227. <https://doi.org/10.3390/ijms20205227>
- Al-Mashhadi, S., Simpson, J. E., Heath, P. R., Dickman, M., Forster, G., Matthews, F. E., Brayne, C., Ince, P. G., Wharton, S. B., & Medical Research Council Cognitive Function and Ageing Study. (2015). Oxidative glial cell damage associated with white matter lesions in the aging human brain. *Brain Pathology (Zurich, Switzerland)*, *25*(5), 565–574. <https://doi.org/10.1111/bpa.12216>
- Alvira, D., Yeste-Velasco, M., Folch, J., Casadesús, G., Smith, M. A., Pallàs, M., & Camins, A. (2007). Neuroprotective effects of caffeine against complex I inhibition-induced apoptosis are mediated by inhibition of the ATM/p53/E2F-1 path in cerebellar granule neurons. *Journal of Neuroscience Research*, *85*(14), 3079–3088. <https://doi.org/10.1002/jnr.21427>
- Barrio-Alonso, E., Hernández-Vivanco, A., Walton, C. C., Perea, G., & Frade, J. M. (2018). Cell cycle reentry triggers hyperploidy and synaptic dysfunction followed by delayed cell death in differentiated cortical neurons. *Scientific Reports*, *8*, 14316. <https://doi.org/10.1038/s41598-018-32708-4>
- Bassermann, F., Frescas, D., Guardavaccaro, D., Busino, L., Peschiaroli, A., & Pagano, M. (2008). The Cdc14B-Cdh1-Plk1 axis controls the G2 DNA-damage-response checkpoint. *Cell*, *134*(2), 256–267. <https://doi.org/10.1016/j.cell.2008.05.043>
- Bender, A., Krishnan, K. J., Morris, C. M., Taylor, G. A., Reeve, A. K., Perry, R. H., Jaros, E., Hershenson, J. S., Betts, J., Klopstock, T., Taylor, R. W., & Turnbull, D. M. (2006). High levels of mitochondrial DNA deletions in substantia nigra neurons in aging and Parkinson disease. *Nature Genetics*, *38*, 515–517. <https://doi.org/10.1038/ng1769>
- Bogdanov, M., Brown, R. H. Jr., Matson, W., Smart, R., Hayden, D., O'Donnell, H., Flint Beal, M., & Cudkowicz, M. (2000). Increased oxidative damage to DNA in ALS patients. *Free Radical Biology and Medicine*, *29*(7), 652–658. [https://doi.org/10.1016/S0891-5849\(00\)00349-X](https://doi.org/10.1016/S0891-5849(00)00349-X)
- Bradley-Whitman, M. A., Timmons, M. D., Beckett, T. L., Murphy, M. P., Lynn, B. C., & Lovell, M. A. (2014). Nucleic acid oxidation: An early feature of Alzheimer's disease.

- Journal of Neurochemistry*, 128, 294–304. <https://doi.org/10.1111/jnc.12444>
- Burma, S., Chen, B. P., Murphy, M., Kurimasa, A., & Chen, D. J. (2001). ATM phosphorylates histone H2AX in response to DNA double-strand breaks. *The Journal of Biological Chemistry*, 276(45), 42462–42467. <https://doi.org/10.1074/jbc.C100466200>
- Cavill, R., Kamburov, A., Ellis, J. K., Athersuch, T. J., Blagrove, M. S. C., Herwig, R., Ebbels, T. M. D., & Keun, H. C. (2011). Consensus-phenotype integration of transcriptomic and metabolomic data implies a role for metabolism in the chemosensitivity of tumour cells. *PLoS Computational Biology*, 7(3), e1001113. <https://doi.org/10.1371/journal.pcbi.1001113>
- Dringen, R., Kussmaul, L., Gutterer, J. M., Hirrlinger, J., & Hamprecht, B. (1999). The glutathione system of peroxide detoxification is less efficient in neurons than in astroglial cells. *Journal of Neurochemistry*, 72(6), 2523–2530. <https://doi.org/10.1046/j.1471-4159.1999.0722523.x>
- Dringen, R., Pawlowski, P. G., & Hirrlinger, J. (2005). Peroxide detoxification by brain cells. *Journal of Neuroscience Research*, 79, 157–165. <https://doi.org/10.1002/jnr.20280>
- Fadul, M. M., Heath, P. R., Cooper-Knock, J., Kurz, J. M., al-Azzawi, H. A., Ali, Z., Smith, T., Matthews, F. E., Brayne, C., Wharton, S. B., & Simpson, J. E. (2020). Transcriptomic analysis of age-associated periventricular lesions reveals dysregulation of the immune response. *International Journal of Molecular Sciences*, 21(21), 7924. <https://doi.org/10.3390/ijms21217924>
- Fakouri, N. B., Hou, Y., Demarest, T. G., Christiansen, L. S., Okur, M. N., Mohanty, J. G., Croteau, D. L., & Bohr, V. A. (2019). Toward understanding genomic instability, mitochondrial dysfunction and aging. *FEBS Journal*, 286, 1058–1073. <https://doi.org/10.1111/febs.14663>
- Ferrante, R. J., Browne, S. E., Shinobu, L. A., Bowling, A. C., Baik, M. J., MacGarvey, U., Kowall, N. W., Brown, R. H. Jr., & Beal, M. F. (1997). Evidence of increased oxidative damage in both sporadic and familial amyotrophic lateral sclerosis. *Journal of Neurochemistry*, 69(5), 2064–2074. <https://doi.org/10.1046/j.1471-4159.1997.69052064.x>
- Frambach, S. J. C. M., van de Wal, M. A. E., van den Broek, P. H. H., Smeitink, J. A. M., Russel, F. G. M., de Haas, R., & Schirris, T. J. J. (2020). Effects of clofibrate and KH176 on life span and motor function in mitochondrial complex I-deficient mice. *Biochimica et Biophysica Acta - Molecular Basis of Disease*, 1866, 165727. <https://doi.org/10.1016/j.bbadis.2020.165727>
- Gatt, A. P., Duncan, O. F., Attems, J., Francis, P. T., Ballard, C. G., & Bateman, J. M. (2016). Dementia in Parkinson's disease is associated with enhanced mitochondrial complex I deficiency. *Movement Disorders*, 31, 352–359. <https://doi.org/10.1002/mds.26513>
- Golubitzky, A., Dan, P., Weissman, S., Link, G., Wikstrom, J. D., & Saada, A. (2011). Screening for active small molecules in mitochondrial complex I deficient patient's fibroblasts, reveals AICAR as the most beneficial compound. *PLoS ONE*, 6, e26883. <https://doi.org/10.1371/journal.pone.0026883>
- Guo, Z., Kozlov, S., Lavin, M. F., Person, M. D., & Paull, T. T. (2010). ATM activation by oxidative stress. *Science*, 330, 517–521. <https://doi.org/10.1126/science.1192912>
- Herrero-Mendez, A., Almeida, A., Fernández, E., Maestre, C., Moncada, S., & Bolaños, J. P. (2009). The bioenergetic and antioxidant status of neurons is controlled by continuous degradation of a key glycolytic enzyme by APC/C-Cdh1. *Nature Cell Biology*, 11(6), 747–752. <https://doi.org/10.1038/ncb1881>
- Isobe, C., Abe, T., & Terayama, Y. (2010). Levels of reduced and oxidized coenzyme Q-10 and 8-hydroxy-2'-deoxyguanosine in the cerebrospinal fluid of patients with living Parkinson's disease demonstrate that mitochondrial oxidative damage and/or oxidative DNA damage contributes to the neurodegeneration. *Neuroscience Letters*, 469, 159–163. <https://doi.org/10.1016/j.neulet.2009.11.065>
- Jacobsen, E., Beach, T., Shen, Y., Li, R., & Chang, Y. (2004). Deficiency of the Mre11 DNA repair complex in Alzheimer's disease brains. *Molecular Brain Research*, 128, 1–7. <https://doi.org/10.1016/j.molbrainres.2004.05.023>
- Jurk, D., Wang, C., Miwa, S., Maddick, M., Korolchuk, V., Tzolou, A., Gonos, E. S., Thrasivoulou, C., Jill Saffrey, M., Cameron, K., & von Zglinicki, T. (2012). Postmitotic neurons develop a p21-dependent senescence-like phenotype driven by a DNA damage response. *Aging Cell*, 11(6), 996–1004. <https://doi.org/10.1111/j.1474-9726.2012.00870.x>
- Kamburov, A., Cavill, R., Ebbels, T. M. D., Herwig, R., & Keun, H. C. (2011). Integrated pathway-level analysis of transcriptomics and metabolomics data with IMPaLA. *Bioinformatics*, 27(20), 2917–2918. <https://doi.org/10.1093/bioinformatics/btr499>
- Keeney, P. M., Xie, J., Capaldi, R. A., & Bennett, J. P. Jr. (2006). Parkinson's disease brain mitochondrial complex I has oxidatively damaged subunits and is functionally impaired and misassembled. *Journal of Neuroscience*, 26, 5256–5264. <https://doi.org/10.1523/JNEUROSCI.0984-06.2006>
- Kim, B. W., Jeong, Y. E., Wong, M., & Martin, L. J. (2020). DNA damage accumulates and responses are engaged in human ALS brain and spinal motor neurons and DNA repair is activatable in iPSC-derived motor neurons with SOD1 mutations. *Acta Neuropathologica Communications*, 8, 7. <https://doi.org/10.1186/s40478-019-0874-4>
- Kinner, A., Wu, W., Staudt, C., & Iliakis, G. (2008). Gamma-H2AX in recognition and signaling of DNA double-strand breaks in the context of chromatin. *Nucleic Acids Research*, 36, 5678–5694. <https://doi.org/10.1093/nar/gkn550>
- Konishi, Y. (2004). Cdh1-APC controls axonal growth and patterning in the mammalian brain. *Science*, 303(5660), 1026–1030. <https://doi.org/10.1126/science.1093712>
- Kraytsberg, Y., Kudryavtseva, E., McKee, A. C., Geula, C., Kowall, N. W., & Khrapko, K. (2006). Mitochondrial DNA deletions are abundant and cause functional impairment in aged human substantia nigra neurons. *Nature Genetics*, 38, 518–520. <https://doi.org/10.1038/ng1778>
- Kruman, I. I., Wersto, R. P., Cardozo-Pelaez, F., Smilenov, L., Chan, S. L., Chrest, F. J., Emokpae, R. Jr., Gorospe, M., & Mattson, M. P. (2004). Cell cycle activation linked to neuronal cell death initiated by DNA damage. *Neuron*, 41(4), 549–561. [https://doi.org/10.1016/S0896-6273\(04\)00017-0](https://doi.org/10.1016/S0896-6273(04)00017-0)
- Liu, S., Bekker-Jensen, S., Mailand, N., Lukas, C., Bartek, J., & Lukas, J. (2006). Claspin operates downstream of TopBP1 to direct ATR signaling towards Chk1 activation. *Molecular and*

- Cellular Biology*, 26(16), 6056–6064. <https://doi.org/10.1128/ MCB.00492-06>
- Lotharius, J. (2005). Progressive degeneration of human mesencephalic neuron-derived cells triggered by dopamine-dependent oxidative stress is dependent on the mixed-lineage kinase pathway. *Journal of Neuroscience*, 25(27), 6329–6342. <https://doi.org/10.1523/JNEUROSCI.1746-05.2005>
- Lotharius, J., Barg, S., Wiekop, P., Lundberg, C., Raymon, H. K., & Brundin, P. (2002). Effect of mutant α -synuclein on dopamine homeostasis in a new human mesencephalic cell line. *Journal of Biological Chemistry*, 277(41), 38884–38894. <https://doi.org/10.1074/jbc.M205518200>
- Lu, T., Pan, Y., Kao, S. Y., Li, C., Kohane, I., Chan, J., & Yankner, B. A. (2004). Gene regulation and DNA damage in the ageing human brain. *Nature*, 429(6994), 883–891. <https://doi.org/10.1038/nature02661>
- Manczak, M., Kandimalla, R., Yin, X., & Reddy, P. H. (2019). Mitochondrial division inhibitor 1 reduces dynamin-related protein 1 and mitochondrial fission activity. *Human Molecular Genetics*, 28, 177–199. <https://doi.org/10.1093/hmg/ddy335>
- Mertens, J., Paquola, A. C. M., Ku, M., Hatch, E., Böhnke, L., Ladjevardi, S., McGrath, S., Campbell, B., Lee, H., Herdy, J. R., Gonçalves, J. T., Toda, T., Kim, Y., Winkler, J., Yao, J., Hetzer, M. W., & Gage, F. H. (2015). Directly reprogrammed human neurons retain aging-associated transcriptomic signatures and reveal age-related nucleocytoplasmic defects. *Cell Stem Cell*, 17(6), 705–718. <https://doi.org/10.1016/j.stem.2015.09.001>
- Moiola, C., de Luca, P., Cotignola, J., Gardner, K., Vazquez, E., & de Siervi, A. (2012). Dynamic coregulatory complex containing BRCA1, E2F1 and CtIP controls ATM transcription. *Cellular Physiology and Biochemistry*, 30, 596–608. <https://doi.org/10.1159/000341441>
- Mortiboys, H., Aasly, J., & Bandmann, O. (2013). Ursocholic acid rescues mitochondrial function in common forms of familial Parkinson's disease. *Brain*, 136, 3038–3050. <https://doi.org/10.1093/brain/awt224>
- Mullaart, E., Boerrigter, M. E. T. I., Ravid, R., Swaab, D. F., & Vijg, J. (1990). Increased levels of DNA breaks in cerebral cortex of Alzheimer's disease patients. *Neurobiology of Aging*, 11, 169–173. [https://doi.org/10.1016/0197-4580\(90\)90542-8](https://doi.org/10.1016/0197-4580(90)90542-8)
- Murata, T., Ohtsuka, C., & Terayama, Y. (2008). Increased mitochondrial oxidative damage and oxidative DNA damage contributes to the neurodegenerative process in sporadic amyotrophic lateral sclerosis. *Free Radical Research*, 42(3), 221–225. <https://doi.org/10.1080/10715760701877262>
- Otsuka, Y., Tanaka, T., Uchida, D., Noguchi, Y., Saeki, N., Saito, Y., & Tatsuno, I. (2004). Roles of cyclin-dependent kinase 4 and p53 in neuronal cell death induced by doxorubicin on cerebellar granule neurons in mouse. *Neuroscience Letters*, 365(3), 180–185. <https://doi.org/10.1016/j.neulet.2004.04.083> <https://doi.org/10.1016/S0304394004005488> [pii]
- Paull, T. T., Rogakou, E. P., Yamazaki, V., Kirchgessner, C. U., Gellert, M., & Bonner, W. M. (2000). A critical role for histone H2AX in recruitment of repair factors to nuclear foci after DNA damage. *Current Biology*, 10(15), 886–895. [https://doi.org/10.1016/S0960-9822\(00\)00610-2](https://doi.org/10.1016/S0960-9822(00)00610-2)
- Petermann, E., & Caldecott, K. W. (2006). Evidence that the ATR/Chk1 pathway maintains normal replication fork progression during unperturbed S phase. *Cell Cycle*, 5, 2203–2209. <https://doi.org/10.4161/cc.5.19.3256>
- Ratcliffe, L. E., Vázquez Villaseñor, I., Jennings, L., Heath, P. R., Mortiboys, H., Schwartzentruber, A., Karyka, E., Simpson, J. E., Ince, P. G., Garwood, C. J., & Wharton, S. B. (2018). Loss of IGF1R in human astrocytes alters complex I activity and support for neurons. *Neuroscience*, 390, 46–59. <https://doi.org/10.1016/j.neuroscience.2018.07.029>
- Rogakou, E. P., Pilch, D. R., Orr, A. H., Ivanova, V. S., & Bonner, W. M. (1998). DNA double-stranded breaks induce histone H2AX phosphorylation on serine 139. *Journal of Biological Chemistry*, 273(10), 5858–5868. <https://doi.org/10.1074/jbc.273.10.5858>
- Sazanov, L. A. (2015). REVIEWS A giant molecular proton pump: Structure and mechanism of respiratory complex I. *Nature Publishing Group*, 16(6), 375–388. <https://doi.org/10.1038/nrm3997>
- Schägger, H., & Pfeiffer, K. (2001). The ratio of oxidative phosphorylation complexes I-V in bovine heart mitochondria and the composition of respiratory chain supercomplexes. *Journal of Biological Chemistry*, 276(41), 37861–37867. <https://doi.org/10.1074/jbc.M106474200>
- Scholz, D., Pörtl, D., Genewsky, A., Weng, M., Waldmann, T., Schildknecht, S., & Leist, M. (2011). Rapid, complete and large-scale generation of post-mitotic neurons from the human LUHMES cell line. *Journal of Neurochemistry*, 119(5), 957–971. <https://doi.org/10.1111/j.1471-4159.2011.07255.x>
- Schwartz, E. I., Smilenov, L. B., Price, M. A., Osredkar, T., Baker, R. A., Ghosh, S., Shi, F. D., Vollmer, T. L., Lencinas, A., Stearns, D. M., Gorospe, M., & Kruman, I. I. (2007). Cell cycle activation in postmitotic neurons is essential for DNA repair. *Cell Cycle*, 6(3), 318–329. <https://doi.org/10.4161/cc.6.3.3752>
- Shanbhag, N. M., Evans, M. D., Mao, W., Nana, A. L., Seeley, W. W., Adame, A., Rissman, R. A., Masliah, E., & Mucke, L. (2019). Early neuronal accumulation of DNA double strand breaks in Alzheimer's disease. *Acta Neuropathologica Communications*, 7, 77. <https://doi.org/10.1186/s40478-019-0723-5>
- Sharma, V., Collins, L. B., Chen, T. H., Herr, N., Takeda, S., Sun, W., Swenberg, J. A., & Nakamura, J. (2016). Oxidative stress at low levels can induce clustered DNA lesions leading to NHEJ mediated mutations. *Oncotarget*, 7(18), 25377–25390. <https://doi.org/10.18632/oncotarget.8298>
- Shi, J., Chen, X., Li, H., Wu, Y., Wang, S., Shi, W., Chen, J., & Ni, Y. (2017). Neuron-autonomous transcriptome changes upon ischemia/reperfusion injury. *Scientific Reports*, 7, 5800. <https://doi.org/10.1038/s41598-017-05342-9>
- Silva, A. R., Santos, A. C., Farfel, J. M., Grinberg, L. T., Ferretti, R. E., Campos, A. H., Cunha, I. W., Begnami, M. D., Rocha, R. M., Carraro, D. M., & de Bragança Pereira, C. A. (2014). Repair of oxidative DNA damage, cell-cycle regulation and neuronal death may influence the clinical manifestation of Alzheimer's disease. *PLoS ONE*, 9(6), e99897. <https://doi.org/10.1371/journal.pone.0099897>
- Simpson, J. E., Ince, P. G., Matthews, F. E., Shaw, P. J., Heath, P. R., Brayne, C., Garwood, C., Higginbottom, A., Wharton, S. B., & MRC Cognitive Function and Ageing Neuro-pathology Study Group. (2015). A neuronal DNA damage response is detected at the earliest stages of Alzheimer's

- neuropathology and correlates with cognitive impairment in the Medical Research Council's Cognitive Function and Ageing Study ageing brain cohort. *Neuropathology and Applied Neurobiology*, 41, 483–496. <https://doi.org/10.1111/nan.12202>
- Simpson, J. E., Ince, P. G., Minett, T., Matthews, F. E., Heath, P. R., Shaw, P. J., Goodall, E., Garwood, C. J., Ratcliffe, L. E., Brayne, C., Rattray, M., Wharton, S. B., & the MRC Cognitive Function and Ageing Neuropathology Study Group. (2016). Neuronal DNA damage response-associated dysregulation of signalling pathways and cholesterol metabolism at the earliest stages of Alzheimer-type pathology. *Neuropathology and Applied Neurobiology*, 42, 167–179. <https://doi.org/10.1111/nan.12252>
- Simpson, J. E., Ince, P. G., Shaw, P. J., Heath, P. R., Raman, R., Garwood, C. J., Gelsthorpe, C., Baxter, L., Forster, G., Matthews, F. E., Brayne, C., Wharton, S. B., & MRC Cognitive Function and Ageing Neuropathology Study Group. (2011). Microarray analysis of the astrocyte transcriptome in the aging brain: Relationship to Alzheimer's pathology and APOE genotype. *Neurobiology of Aging*, 32(10), 1795–1807. <https://doi.org/10.1016/j.neurobiolaging.2011.04.013>
- Suberbielle, E., Sanchez, P. E., Kravitz, A. V., Wang, X., Ho, K., Eilertson, K., Devidze, N., Kreitzer, A. C., & Mucke, L. (2013). Physiologic brain activity causes DNA double-strand breaks in neurons, with exacerbation by amyloid- β . *Nature Neuroscience*, 16, 613–621. <https://doi.org/10.1038/nn.3356>
- Sudo, T., Ota, Y., Kotani, S., Nakao, M., Takami, Y., Takeda, S., & Saya, H. (2001). Activation of Cdh1-dependent APC is required for G1 cell cycle arrest and DNA damage-induced G2 checkpoint in vertebrate cells. *EMBO Journal*, 20(22), 6499–6508. <https://doi.org/10.1093/emboj/20.22.6499>
- Tang, Y., Liu, M. L., Zang, T., & Zhang, C. L. (2017). Direct reprogramming rather than iPSC-based reprogramming maintains aging hallmarks in human motor neurons. *Frontiers in Molecular Neuroscience*, 10, 359. <https://doi.org/10.3389/fnmol.2017.00359>
- Tomashevski, A., Webster, D. R., Grammas, P., Gorospe, M., & Kruman, I. I. (2010). Cyclin-C-dependent cell-cycle entry is required for activation of non-homologous end joining DNA repair in postmitotic neurons. *Cell Death and Differentiation*, 17(7), 1189–1198. <https://doi.org/10.1038/cdd.2009.221>
- Ward, I. M., & Chen, J. (2001). Histone H2AX is phosphorylated in an ATR-dependent manner in response to replicational stress. *Journal of Biological Chemistry*, 276(51), 47759–47762. <https://doi.org/10.1074/jbc.C100569200>

SUPPORTING INFORMATION

Additional supporting information may be found in the online version of the article at the publisher's website.

How to cite this article: Vazquez-Villasenor, I., Garwood, C. J., Simpson, J. E., Heath, P. R., Mortiboys, H., & Wharton, S. B. (2021). Persistent DNA damage alters the neuronal transcriptome suggesting cell cycle dysregulation and altered mitochondrial function. *European Journal of Neuroscience*, 1–19. <https://doi.org/10.1111/ejn.15466>